Chinese Journal of Structural Chemistry

ARTICLE

Acid-Stable $CoWO_4/WO_3$-Microrod Coated by a Thin Carbon-Layer as Efficient Pt Co-Catalysts for Methanol Oxidation and Oxygen Reduction

Jiahuan Li[1], Jiahao Xie[1], Xinyu Wang[1], Ying Dai[2]*, Xiaoqin Xu[1], Jin Liu[1], Zhuang Cai[1]*, Xin Meng[1] and Jinlong Zou[1]*

[1]*Key Laboratory of Functional Inorganic Material Chemistry, Ministry of Education of the People's Republic of China, School of Chemistry and Materials Science, Heilongjiang University, Harbin 150080, China*

[2]*School of Civil Engineering, Heilongjiang Institute of Technology, Harbin 150050, China*

ABSTRACT Insufficient activity and instability (poisoning) of Pt-based electrocatalysts for methanol oxidation and oxygen reduction reactions (MOR/ORR) impede the development of direct methanol fuel cells. Here, $CoWO_4$ nanoparticles-loaded WO_3 microrods coated by a thin carbon-layer are used as Pt-supports/co-catalysts for MOR/ORR. WO_3 grows along the (110) crystal plane to form microrod (diameter of ~0.6 um), which is coated by a carbon-layer (~5 nm). Pt-$CoWO_4/WO_3$@NCL-mr (850 ℃) shows a higher mass activity (2208 mA mg^{-1}_{pt}) than the commercial Pt/C (659.4 mA mg^{-1}_{pt}). $CoWO_4/WO_3$ heterojunction on the microrod surface with abundant oxygen vacancies allows the generation of surface-adsorbed hydroxyl to facilitate CO elimination and regeneration of the occupied Pt active-sites (promising stability). Pt-$CoWO_4/WO_3$@NCL-mr (850 ℃) has higher half-wave (0.46 V) and onset (0.54 V) potentials than Pt/C (0.41 and 0.50 V) for ORR. The microrod structure of $CoWO_4/WO_3$@NCL facilitates the dispersibility of Pt NPs to increase the utilization of Pt active sites and relieve the self-aggregation of Pt to obtain a promising synergy between Pt and $CoWO_4$ (Co^{2+}) for ORR in acid media. This study provides insights not only into the synthesis of acid-resistant WO_3@NCL microrod as active Pt co-catalyst, but also into the effective utilization of surface oxygen vacancies and Co^{2+} for MOR/ORR.

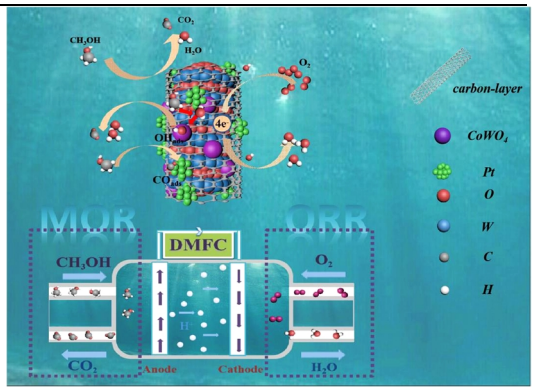

Keywords: acid resistance, methanol-tolerance, oxygen vacancies, strong metal-support interaction, thin carbon-layer

n INTRODUCTION

Throughout the history, energy is always the essential factor for development.[1] At present, most of countries (including developed and less-developed countries) still use traditional fossil fuels such as oil, coal and natural gas to meet the electricity demand.[2] The consumption of resources, the deterioration of environment, and the global climate change have forced us to find clean and pollution-free energy sources.[1] Direct methanol fuel cells (DMFCs) as a viable alternative have considerable advantages including low cost and friendly environment, consistent with the sustainable development strategies.[2,3] It is known that Pt-based materials are generally used in DMFCs as both methanol oxidation reaction (MOR) and oxygen reduction reaction (ORR) catalysts.[3-5] In the case where the roles of Pt-based catalysts (monoatomic Pt or Pt nanoparticle (NPs)) are still irreplaceable (such as MOR), we should do more to explore the catalyst with a low Pt loading.[6-10]

Transition metal compounds have long been served as catalyst/co-catalyst to increase the Pt utilization to gain superior MOR/ORR activity. Tungsten (W) compounds including $CoWO_4$ and WO_3 have shown the promising activities in many fields including photocatalysis (photocatalytic degradation or hydrogen evolution),[11-14] photodetectors,[15] fuel cells,[16] supercapacitors,[17,18] and sensors (acetone or NH_3 gas sensing).[19,20] It has been reported that transition metal oxides (TMOs) can help Pt-based catalyst to reduce the CO poisoning in the MOR process,[21] because the strong metal-support interaction (SMSI) between Pt and TMOs can greatly improve the MOR activity and stability.[22,23] Among various TMOs, WO_3 usually exhibits a high oxygen storage capacity, a good corrosion resistance in acid medium, and a variable W valence, which can facilitate the adsorption of OH_{ads} on the Pt surface to promote the CO oxidation during MOR.[21,22]

The poor conductivity of WO_3 limits its charge-transfer capacity, and therefore, it is interesting to combine WO_3 with the highly-conductive materials such as carbon materials to further improve the catalytic activity and CO resistance of Pt-based catalysts. Georgieva et al. prepare the graphite-supported $Pt/TiO_2/WO_3$ catalyst by using deposition method, which is 5 times more active than Pt/WO_3 for MOR under visible light.[24] Madhu et al. use $W_{18}O_{49}$ nanowires grown on carbon paper as the Pt support/co-catalyst for proton exchange membrane fuel cell, and $Pt/W_{18}O_{49}$/carbon paper composite with the three-dimensional structure shows the higher ORR activity and CO toxicity resistance than Pt/C.[25] Ye et al. prepare the Pt/WO_3-C catalyst by using the microwave pyrolysis method, which can improve the Pt NPs distribution and electrochemical surface area to enhance the MOR activity.[26] Note that the high activity is also attributed to the uniform dispersion of WO_3 on carbon.[26] Furthermore, it is worth to note that wolframite-

© 2022 fjirsm, CAS, Fuzhou

DOI: 10.14102/j.cnki.0254-5861.2022-0104

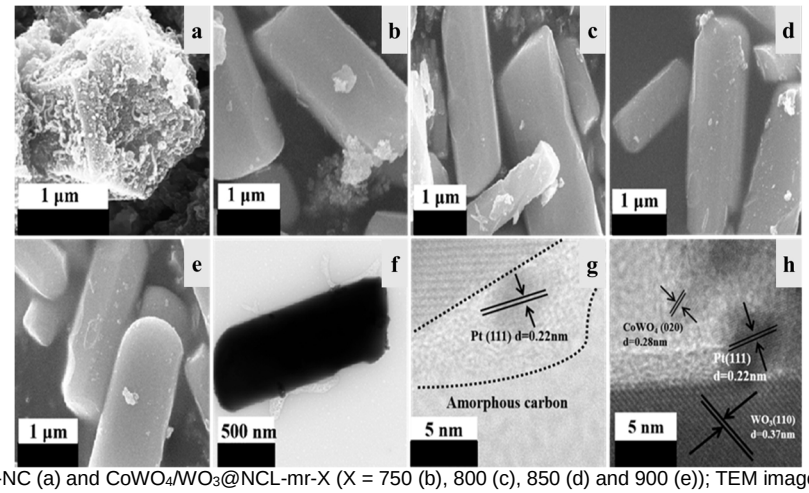

Figure 1. SEM images of Co-NC (a) and $CoWO_4/WO_3$@NCL-mr-X (X = 750 (b), 800 (c), 850 (d) and 900 (e)); TEM image (f) and high-resolution TEM images (g and h) of Pt-$CoWO_4/WO_3$@NCL-mr-850.

type $CoWO_4$ belonging to a monoclinic crystal structure is a well-known electroactive material.[24-26] The nano-structure of $CoWO_4$ usually has the high thermal stability and electrical conductivity.[27] However, its charge transfer resi tance s still needs to be lowered to improve the catalytic stability and activity. Therefore, the combination between W-compounds (WO_3/$CoWO_4$) and conductive carbon may be a feasible way to prepare the Pt support/co-catalyst.

In this study, zeolitic imidazolate framework (ZIF)-8@ZIF-67 material is synthesized as carbon and Co sources to prepare the Co-species embedded nitrogen-doped carbon (Co-NC). The mixture of ammonium tungstate and Co-NC is carbonized to obtain the WO_3@N-doped carbon layer (WO_3@NCL micro-rods) to support the $CoWO_4$ NPs ($CoWO_4/WO_3$@NCL-mr). It is the first time to use $CoWO_4/WO_3$@NCL-mr catalysts as the Pt-supports/co-catalyst for MOR/ORR. WO_3 is grown directionally along the (110) crystal plane to form the micrometer-sized rod. By carbonization at high temperature, WO_3-mr is covered by a carbon thin-layer (~5 nm) derived from NC to protect the oxygen vacancies and active sites on the surface of WO_3. $CoWO_4$ NPs are derived from the combination of Co and W species, which are firmly anchored on the surface of WO_3@NCL-mr. Due to the largely-exposed surface of micro-rod, Pt NPs can be well dispersed on the surface of $CoWO_4/WO_3$@NCL-mr to increase the exposure of Pt active sites. As expected, the resistance to CO (MOR) or methanol (methanol penetration, ORR) poisoning, as well as the MOR/ORR activity of Pt-$CoWO_4/WO_3$@NCL-mr catalysts, is much higher than those of commercial Pt/C in acidic electrolytes.

n RESULTS AND DISCUSSION

Composition and Structure Characterizations of $CoWO_4/WO_3$@NCL-mr. Morphology and structure of the synthesized samples are elucidated by scanning electron microscopy (SEM) and transmission electron microscopy (TEM) images. Figure 1a shows the morphology of Co-NC obtained from the carbonization of ZIF-8@ZIF-67 polyhedron at 900 °C. Figure 1b-1e show the SEM images of $CoWO_4/WO_3$@NCL-mr-X (X = 750, 800, 850 and 900), which indicate that the micro-rods orienting along the (110) crystal plane of WO_3 are formed. The formation of micro-rods is ascribed to two reasons including Oswald ripening and Kirkendall effects.[28-30] With the addition of W sources, the dodecahedral structure of Co-NC completely disappears. Co-NC is decomposed to form the carbon layer to coat on the surface of WO_3-mr, and the Co atoms are combined with W atoms to generate the $CoWO_4$ NPs. As shown in Figure 1f, $CoWO_4/WO_3$@ NCL-mr-850 has the micro-rod shape with a length of ~1.5 um and a diameter of ~0.6 um. In Figure 1g and 1h, the lattice fringes of $CoWO_4$, WO_3, and Pt can be clearly observed (HRTEM images). As Figure 1g depicts, there is an obvious carbon thin-layer (~5 nm) coated on the surface of WO_3-mr, which can protect the oxygen vacancies and active sites on WO_3-mr. The carbon layer is gene rated by the pyrolysis (decomposition) of NC.[31] In Figure 1h, the micro-rod-shaped body is WO_3 with the monoclinic structure and attachment of $CoWO_4$ and Pt NPs,[32] and the lattice spacing of 0.37, 0.28, 0.22 nm corresponds to the crystal planes of WO_3 (110), $CoWO_4$ (020) and Pt (111), respectively.

Figure 2 shows the X-ray diffraction (XRD) patterns of the $CoWO_4/WO_3$@NCL-mr composites before and after Pt loading. In Figure 2a, four characteristic diffraction peaks of $CoWO_4/WO_3$@ NCL-mr-X (X = 750, 800, 850, and 900) at around 24.0°, 28.2°, 33.1°, and 34.0° correspond to the (110), (101), (111) and (200) crystal planes of WO_3 (JCPDS, 05-0388), respectively. Other peaks can be classified as the wolframite-type monoclinic $CoWO_4$ crystal [space group *P*2/a (13)] (JCPDS, 15-0867).[33,34] In Figure

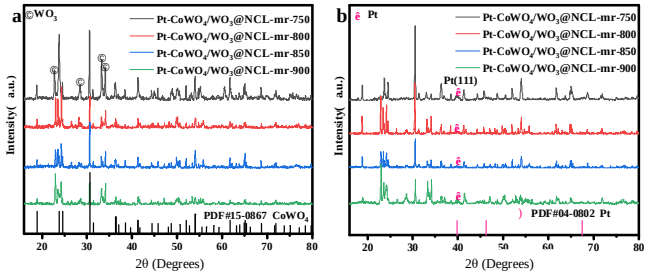

Figure 2. XRD patterns of $CoWO_4/WO_3$@NCL-mr-X (a) and Pt-$CoWO_4/WO_3$@NCL-mr-X (b) (X = 750, 800, 850 and 900).

© 2022 fjirsm, CAS, Fuzhou
Chin. J. Struct. Chem. **2022**, 41, 2207059-2207067
DOI: 10.14102/j.cnki.0254-5861.2022-0104

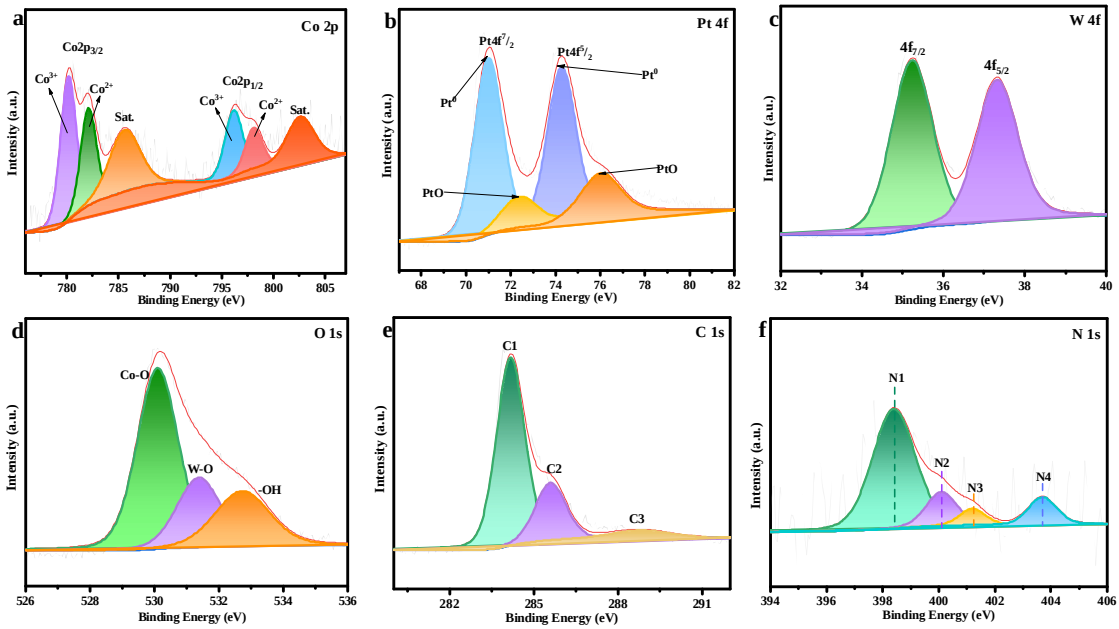

Figure 3. High-resolution XPS spectra of Co 2p (a), Pt 4f (b), W 4f (c), O 1s (d), C 1s (e) and N 1s (f) for Pt-$CoWO_4$/WO_3@NCL-mr-850.

2b, the diffraction signal of Pt can be clearly observed at around 39.7°, corresponding to the (111) crystal plane of Pt (JCPDS, 04-0802). These peaks match well with the standard cards and there are no other impurities, indicating that only WO_3 and $CoWO_4$ coexist in the catalysts, in agreement with TEM results. The XRD patterns do not show a graphic carbon peak, indicating that WO_3-mr and/or $CoWO_4$ NPs should be wrapped by the amorphous carbon-layer.

The chemical compositions of Pt-$CoWO_4$/WO_3@NCL-mr catalysts are characterized by X-ray photoelectron spectroscopy (XPS) (Figure 3 and Figure S1-S7). As expected, Co 2p, Pt 4f, W 4f, O 1s, C 1s and N 1s are observed in the catalysts. The high-resolution XPS spectra of Co 2p (Figure 3a and Figure S1) exhibit two peaks at around 780.9 (Co $2p_{3/2}$) and 796.5 (Co $2p_{1/2}$) eV, corresponding to the characteristic peaks of Co^{2+}.[35,36] The other two peaks at around 786.3 and 802.8 eV are the satellite peaks for Co $2p_{3/2}$ and Co $2p_{1/2}$ (marked as "sat."), respectively.[35,37,38] Figure 3b shows that the Pt species has been successfully deposited on the $CoWO_4$/WO_3@NCL-mr support. The Pt 4f spectra can be classified as the double peaks from the spin-orbit splitting of Pt $4f_{7/2}$ and Pt $4f_{5/2}$ (Figure 3b and Figure S2). The strongest doublet (at around 71.0 and 74.2 eV) belongs to the metallic Pt (Pt^0), while the other doublet (at around 72.4 and 76.0 eV) corresponds to the PtO (Pt II).[36] The main peaks are basically ascribed to Pt^0, indicating that the SMSI between Pt and $CoWO_4$/WO_3@NCL-mr can well protect the Pt active sites from deactivation (oxidation).[36] In addition, the percentage contents of Pt^0 and PtO in Pt/C and Pt-$CoWO_4$/WO_3@NCL-mr-X (X = 750, 800, 850 and 900) are shown in Figure S3, indicating that Pt^0 is the main species in these catalysts. The catalytic activity of Pt is mainly determined by Pt^0, followed by Pt II.[36] Figure 3c and Figure S4 are the high-resolution XPS spectra of W4f. The spectra of W 4f indicates the presence of W in two chemical states ($CoWO_4$ and WO_3), and two sets of double peaks corresponding to W $4f_{7/2}$ and W $4f_{5/2}$ (W^{6+}) can be observed.[35,37,38] The peaks at 35.2±0.1 and 35.8±0.1 eV correspond to the W $4f_{7/2}$, while the peaks at 37.4±0.2 and 38.3±0.1 eV correspond to the W $4f_{5/2}$.[35] Therefore, the XPS results confirm the successful formation of $CoWO_4$ and WO_3 or $CoWO_4$/WO_3 heterojunction (as shown in TEM image), which can promote the charge transfer to improve the ORR activity.

Figure 3d and Figure S5 show the deconvolution peaks of O 1s spectra. The three peaks correspond to O^{2-} ion in WO_4 root, WO_3, and the oxygen ions in -OH adsorbed on the surface of the materials, which are located at around 530.1 (O^{2-}) and 531.38 (W-O) and 532.73 eV (-OH), respectively.[34] The high-resolution C 1s spectra (Figure 3e and Figure S6) show three peaks including C1, C2, and C3 peaks located at around 284.17, 285.6, and 288.8 eV, respectively. Generally, peak C1 is assigned to the C-C bond corresponding to the amorphous carbon of NCL;[37] peak C2 is attributed to the C-O/C-N, which indicates the existence of N-doped carbon skeleton;[39] and peak C3 corresponds to the O-containing group of O-C=O. The hydrophilic O-groups on the carbon skeleton can promote the adsorption and reduction of oxygen.[40]

Figure 3f and Figure S7 show the high-resolution spectra of N1s, indicating the successful doping of N atoms. The four deconvolution peaks of N 1s are located at around 398.4 (N1), 400±0.3 (N2), 400.7±0.4 (N3) and 403.7 eV (N4), which can be assigned to pyridine-N, pyrrole-N, graphite-N, and oxide-N, respectively.[40-42] As shown in Figure 4a, with the increase of temperature, the N2 contents in Pt-$CoWO_4$/WO_3@NCL-mr catalysts decrease due to the instability of N2 at high temperatures.[43] As previously reported, N1 and N3 are deemed to play important roles in enhancing the ORR catalytic activity.[41-43] N1 can reduce the energy barrier of O_2 adsorption and increase the first electron transfer rate during ORR.[42] N3 can increase the electrical conductivity of catalyst to facilitate the charge transfer.[43] The doping of N atoms in the carbon framework makes the surrounding of carbon atoms more positively charged, which may also facilitate the coating and even-

 © 2022 fjirsm, CAS, Fuzhou
DOI: 10.14102/j.cnki.0254-5861.2022-0104

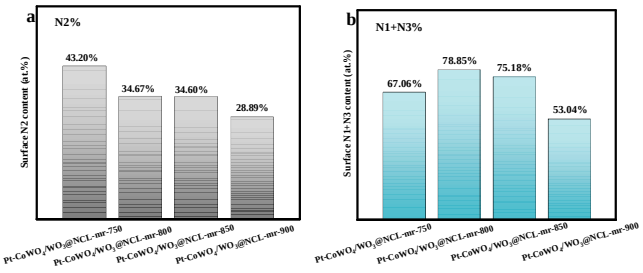

Figure 4. Percentage contents of N2 (a) and N1+N3 (b) in Pt-$CoWO_4/WO_3$@NCL-mr-X (X = 750, 800, 850 and 900).

distribution of Pt NPs on the surface of $CoWO_4/WO_3$@NCL-mr. As shown in Figure 4b, the proportions of N1+N3 in Pt-$CoWO_4/WO_3$@NCL-mr-X (X = 800 and 850) even exceed 75%, which has a positive impact on the enhancement of ORR activity.

MOR Activities of Pt-$CoWO_4/WO_3$/ZNC-CNT Catalysts. Figure 5a shows that the cyclic volammetry (CV) curves of Pt-$CoWO_4/WO_3$@NCL-mr catalysts have obvious hydrogen adsorption/desorption regions, and Pt-$CoWO_4/WO_3$@NCL-mr-850 has the largest H-region area. ECSAs of the catalysts are calculated by using Equation (1), and the results are presented in Table S1. As shown in Table S1, the highest ECSA of 225.8 $m^2\ g^{-1}_{Pt}$ is obtained by Pt-$CoWO_4/WO_3$@NCL-mr-850, which is approximately 1.97 times higher than that of Pt/C (114.47 $m^2\ g^{-1}_{Pt}$). It is generally recognized that the larger the ESCA value, the better the MOR catalytic activity. Therefore, the MOR performance of Pt-$CoWO_4/WO_3$@NCL-mr-850 catalyst is superior to that of Pt/C. MOR activities of the catalysts tested in 0.5 M H_2SO_4 + 0.5 M CH_3OH between -0.2 and 1.0 V are shown in Figure 5b. Pt-$CoWO_4/WO_3$@NCL-mr-850 shows the highest mass activity (2208 mA mg^{-1}_{Pt}) among all of the catalysts, which is 3.34 times higher than that of Pt/C (659.4 mA mg^{-1}_{Pt}). The mass activities of Pt-$CoWO_4/WO_3$@NCL-mr-900 (1700.4 mA mg^{-1}_{Pt}) and Pt-$CoWO_4/WO_3$@NCL-mr-800 (1038.9 mA mg^{-1}_{Pt}) are also higher than that of Pt/C. As shown in Table S2, the mass activity of Pt-$CoWO_4/WO_3$@NCL-mr-850 is much higher than those of most of recently-reported Pt-based catalysts. These results imply that the special structure (the micro-rod shape and N-doped carbon layer) of $CoWO_4/WO_3$@NCL-mr can increase the exposure of Pt active sites to improve the MOR activity, and the synergy and interfacial interaction between $CoWO_4$ and WO_3 can also increase the catalytic activity.[27,44]

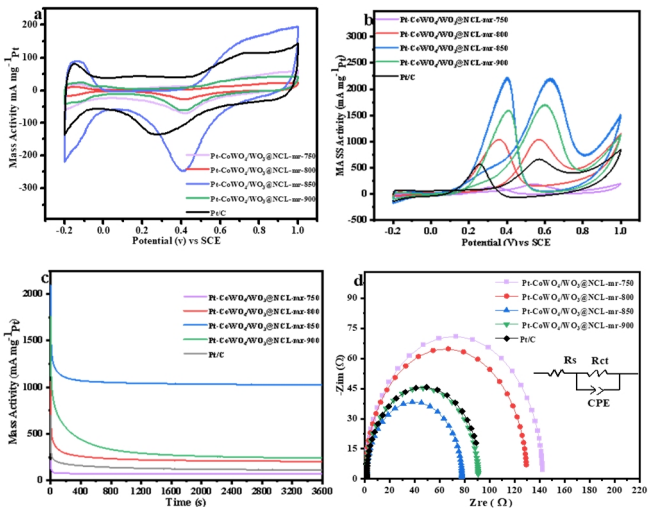

Figure 5. CV curves tested in 0.5 M H_2SO_4 media (a); CV curves tested in 0.5 M H_2SO_4 + 0.5 M CH_3OH (b); Time-current curves at a potential of 0.67 V (c); Nyquist plots measured in 0.5 M H_2SO_4 + 0.5 M CH_3OH for Pt/C and Pt-$CoWO_4/WO_3$@NCL-mr-X (X = 750, 800, 850 and 900) catalysts (d).

Chronogalvanometry (CA) test is an effective method to evaluate the electrocatalytic stability under the steady-state condition. Figure 5c shows the CA curves of Pt-$CoWO_4/WO_3$ @NCL-mr and Pt/C catalysts. After 3600 s, the current densities of Pt/C and Pt-$CoWO_4/WO_3$@NCL-mr-850 are 112.04 and 1023 mA mg^{-1}_{Pt}, respectively. Therefore, the MOR stability of Pt-$CoWO_4/WO_3$@NCL-mr-850 is better than that of Pt/C. Figure 5d shows the Nyquist plots and the equivalent circuit diagram (inset). The semicircular Nyquist plots indicate that the electrode reactions involved are governed by the charge transfer step.[45] The diameter of the arc represents the charge transfer resistance (R_{ct}). The smaller the diameter, the smaller the resistance, and the faster the charge transfer. As Pt-$CoWO_4/WO_3$@NCL-mr-850 (R_{ct} of 77.77 Ω) has smaller diameter of arc than Pt/C (89.02 Ω), it has the fastest charge transfer speed, implying that the hydrogen tungsten bronze (H_xWO_3) with a high electrical conductivity may be generated on WO_3 by combining with hydrogen ion.[46] Moreover, the oxygen vacancies on WO_3 can facilitate the hydrogen ion diffusion for H_xWO_3.[47,48]

To identify the CO tolerance of Pt-$CoWO_4/WO_3$@NCL-mr during MOR, CO stripping tests are performed. In Figure 6, the onset potential of CO oxidation on Pt/C catalyst appears at around 0.54 V, while that for Pt-$CoWO_4/WO_3$@NCL-mr catalysts has significant negative shifts. Therefore, Pt-$CoWO_4/WO_3$@NCL-mr catalysts have high CO oxidation activity (CO poisoning tolerance). Compared with Pt/C, CO on Pt-$CoWO_4/WO_3$@NCL-mr catalysts is more easily removed (oxidized) to release the active sites. As reported previously, W species can provide abundant oxygen species for CO removal.[45,49] In addition, the SMSI between Pt and support greatly promotes the exposure of Pt active sites to thus improve the CO oxidation and MOR activity. In the previous

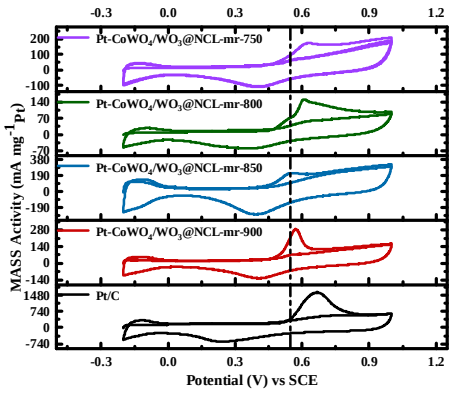

Figure 6. CO stripping voltammograms of Pt/C and Pt-$CoWO_4/WO_3$@NCL-mr-X (X = 750, 800, 850 and 900) catalysts.

© 2022 fjirsm, CAS, Fuzhou
Chin. J. Struct. Chem. **2022**, 41, 2207059-2207067
DOI: 10.14102/j.cnki.0254-5861.2022-0104

reportes, H_xWO_3 may be generated by the spillover effect (desirable) to improve the CO oxidation and charge transfer.[50-52] Note that the CO mobility on different crystal planes may be affected by the number and distribution of the exposed crystal planes,[53] which accordingly affects the CO tolerance of Pt-$CoWO_4/WO_3$@NCL-mr catalysts. $CoWO_4/WO_3$ heterojunction attached on the micro-rod structure of WO_3 with abundant oxygen vacancies allows rapid oxygen transfer along the interfacial channel, thereby enhancing the redox interfacial activity with the generation of surface-adsorbed hydroxyl, which facilitates the quick regeneration (CO elimination) of the occupied Pt active sites to form a clean catalyst for MOR.

As shown in reactions 1-4, CO can be independently adsorbed on $CoWO_4$ ($CoWO_4$-CO_{ads}) and then oxidized by the surface-adsorbed hydroxyl ($CoWO_4$-$(OH)_{ads}$).[46,47] As reported previously, the rearrangement of Co^{2+} ions in $CoWO_4$ and the high proportion of Co^{2+}-ion pairs with a shorter nearest-neighbor distance favor the methanol (including CO) oxidation via the Langmuir-Hinshelwood (L-H) pathway.[32] Therefore, Pt-$CoWO_4/WO_3$@ NCL-mr catalyst has a high resistance to CO poisoning and an outstanding MOR stability. The reaction processes on Pt-$CoWO_4/WO_3$@ NCL-mr catalysts during the anodization are shown below (reactions 1-9). The hydrogen ions in Pt-H are transferred from Pt to WO_3 to form H_xWO_3 to remove hydrogen, which is called the spillover effect.[54,55] According to reactions (8) and (9), the formation of H_xWO_3 makes the dehydrogenation of methanol more effective and helps to remove the adsorbed intermediates during MOR.

$$CoWO_4 + CH_3OH \rightarrow CoWO_4\text{-}CO_{ads} + 4H^+ + 4e^- \quad (1)$$
$$CoWO_4 + H_2O \rightarrow CoWO_4\text{-}H_2O_{ads} \quad (2)$$
$$CoWO_4\text{-}H_2O_{ads} \rightarrow CoWO_4\text{-}(OH)_{ads} + H^+ + e^- \quad (3)$$
$$CoWO_4\text{-}(CO)_{ads} + CoWO_4\text{-}(OH)_{ads} \rightarrow CoWO_4 + CO_2 + H^+ + e^- \quad (4)$$
$$Pt + H_2O \rightarrow Pt\text{-}(OH)_{ads} + H^+ + 4e^- \quad (5)$$
$$Pt\text{-}(CHO)_{ads} + Pt\text{-}(OH)_{ads} \rightarrow 2Pt + CO_2 + 2H^+ + 2e^- \quad (6)$$
$$CH_3OH + H_2O \rightarrow CO_2 + 6H^+ + 6e^- \quad (7)$$
$$Pt\text{-}(CHO)_{ads} + Pt\text{-}(OH)_{ads} + WO_3 \rightarrow 2Pt + CO_2 + H_xWO_3 \quad (8)$$
$$H_xWO_3 \rightarrow WO_3 + xe^- + xH^+ \quad (9)$$

ORR Activities of Pt-$CoWO_4/WO_3$@NCL-mr Catalysts. In Figure 7a, CV tests for Pt-$CoWO_4/WO_3$@NCL-mr and Pt/C catalysts are performed in a 0.5 M H_2SO_4 solution saturated with O_2 at 50 mV s^{-1}. All of the catalysts show obvious oxygen reduction peaks.[56] As shown in Figure 7b, Pt-$CoWO_4/WO_3$@ NCL-mr-850 has higher half-wave (0.46 V) and onset (0.54 V) potentials than Pt/C (0.41 and 0.50 V). The onset potentials, half-wave potentials and limiting current densities of Pt-$CoWO_4/WO_3$@NCL-mr-850 and Pt/C catalysts are listed in Table S3. The promising ORR activity is mainly derived from the cooperation between Pt and Co^{2+} ($CoWO_4$). The surface Co^{2+} as active sites for ORR favors the oxygen adsorption on the catalyst surface to improve the oxygen catalysis. Moreover, the ORR-related intermediate (-OH) on catalyst surface (Co^{2+}) can immediately react with H^+ to form H_2O molecule to release the active sites.[43,57] It is also reported that abundant oxygen vacancies on WO_3 can facilitate the distribution of Pt NPs to enhance the adsorption of O_2 molecules onto the surface adjacent to the exposed Pt active-sites.[56-58] Furthermore, the strong interaction between WO_3 and NCL (with various N species) can greatly smoothen the charge transfer to enhance the ORR activity.[58,59]

Figure 7c and 7d show the linear sweep voltammetry (LSV) curves measured from 400 to 2500 rpm and K-L curves (inset). As the rotation speed increases, the limiting current (j) increases as the oxygen diffusion from electrolyte to the electrode surface increases. All of the electron transfer number (n) is close to 4.0, indicating that both Pt-$CoWO_4/WO_3$@NCL-mr-850 and Pt/C follow the effective 4e- ORR pathway. The rod-like structure (surface)

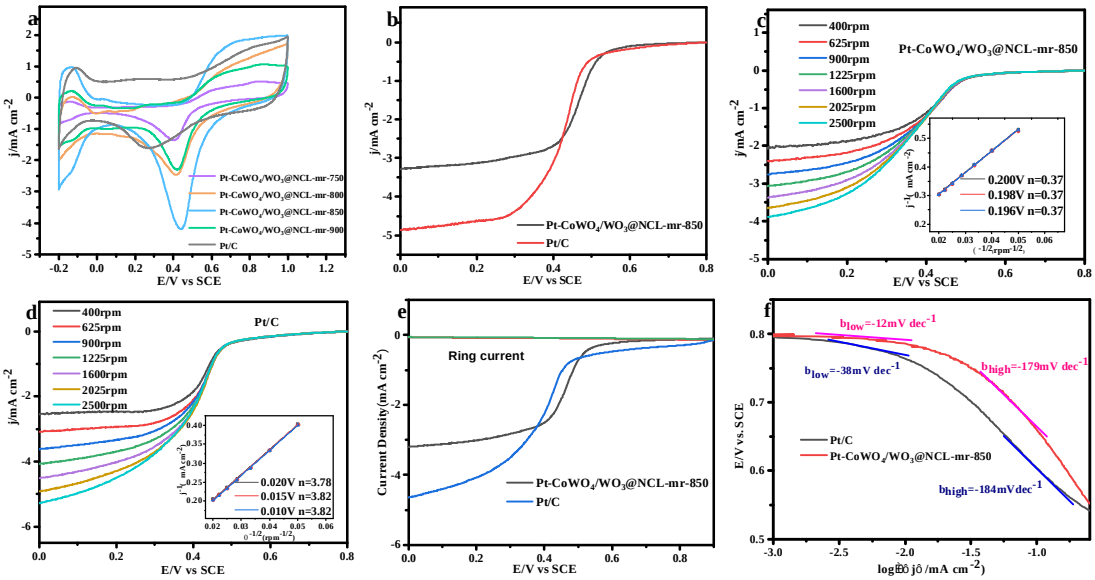

Figure 7. CV curves of Pt-$CoWO_4/WO_3$@NCL-mr-X (X = 750, 800, 850 and 900) and Pt/C (a) catalysts; LSV curves of Pt-$CoWO_4/WO_3$@NCL-mr-850 and Pt/C catalysts in O_2-saturated 0.5 M H_2SO_4 solution at 1600 rpm (10 mV s^{-1}) (b); LSV and calculated K-L plots at different potentials (insets) of Pt-$CoWO_4/WO_3$@NCL-mr-850 (c) and Pt/C (d) catalysts in O_2-saturated 0.5 M H_2SO_4 solution at different rotation rates (10 mV s^{-1}); RRDE tests of the cathodic catalysts (e); Tafel plots of Pt-$CoWO_4/WO_3$@NCL-mr-850 and Pt/C catalysts (f).

 © 2022 fjirsm, CAS, Fuzhou
DOI: 10.14102/j.cnki.0254-5861.2022-0104

of WO_3@NCL-mr can serve abundant Pt-binding sites to promote the exposure of Pt active sites to boost the ORR process. The rotating risk disk electrodes (RRDE) result in Figure 7e further confirms the 4e$^-$ ORR pathway on Pt-$CoWO_4/WO_3$@ NCL-mr-850. In the potential range of 0.0-0.38 V, H_2O_2 yields of Pt-$CoWO_4/WO_3$/ZNC-CNT-850 change from 7.2 to 12.0%. In 0.5 M H_2SO_4 solution, the n values of Pt-$CoWO_4/WO_3$@NCL-mr-850 and Pt/C vary between 3.8 and 3.9 (Figure S8), indicating that both of them possess a high catalytic-selectivity for converting O_2 into OH^- via a 4e$^-$ ORR pathway. Figure 7f shows the Tafel polarization curves in the low and high potential regions. The lower slope usually suggests that the catalyst has a faster ORR kinetics at the electrocatalytic interface at lower potentials.[60] In the two potential regions, the Tafel slopes of Pt-$CoWO_4/WO_3$@NCL-mr-850 are 12 and 179 mV dec^{-1}, which are slightly better than those of Pt/C (38 and 184 mV dec^{-1}). Thereafter, the heterogeneous interfaces among Pt, $CoWO_4$ and WO_3 can eagerly construct smooth pathways for charge transfer (4e$^-$ ORR process),[61] which contributes to a promising ORR kinetics on Pt-$CoWO_4/WO_3$@ NCL-mr-850.[60]

Figure S9 shows the CA and methanol resistance tests for Pt-$CoWO_4/WO_3$@NCL-mr-850 and Pt/C. These two tests are the important index for evaluating the ORR activity of catalysts. Under the same conditions, the stability of Pt-$CoWO_4/WO_3$@NCL-mr-850 is better than that of Pt/C. The protective effect of the N-doped carbon layer (NCL) can maintain the stability of the co-catalytically active-sites on $CoWO_4$ (Co^{2+}).[62] The synergistic effects between Pt and Co^{2+}, as well as spillover effects of the generated H_xWO_3, can accelerate the methanol dehydrogenation to release Pt active sites to thus improve the charge transfer and methanol tolerance (ORR stability) on Pt-$CoWO_4/WO_3$@NCL-mr-850.

Possible Mechanisms for MOR and ORR on Pt-$CoWO_4/WO_3$@NCL-mr Catalysts. Scheme 1 shows the MOR and ORR processes on Pt-$CoWO_4/WO_3$@NCL-mr catalysts. During the MOR process, methanol molecules can be easily adsorbed by O-groups (OH/COOH/COC) on the surface of Pt-$CoWO_4/WO_3$@NCL-mr, which are then oxidized by the dispersed Pt active sites. Meanwhile, the hydrogen overflow effect between Pt and WO_3 facilitates the formation of H_xWO_3 on the WO_3 surface

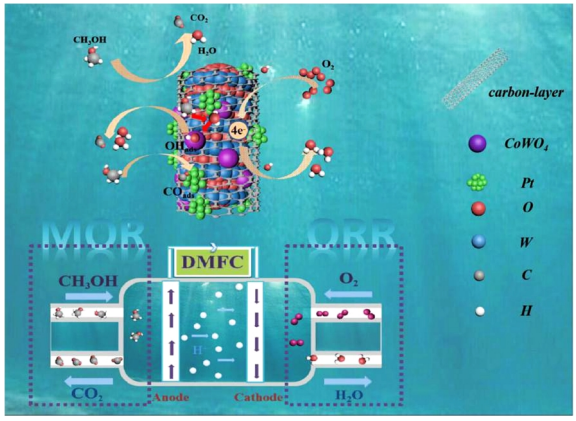

Scheme 1. Schematic diagram of MOR and ORR processes on Pt-$CoWO_4/WO_3$@NCL-mr catalysts.

to enhance the dehydrogenation of methanol molecules by utilizing the oxyphilic nature of oxides,[63] which can facilitate to release the occupied Pt active-sites to further adsorb the methanol molecules. In addition, WO_3-mr (H_xWO_3) and surface-adsorbed hydroxyl ($CoWO_4$-$(OH)_{ads}$) can enhance the removal of intermediates to improve the resistance to CO poisoning (MOR stability) in acidic media.[34,46,47] For ORR, the micro-rod-shaped $CoWO_4/WO_3$ @NCL promotes the dispersibility of Pt NPs to relieve the self-aggregation of Pt, and prevent the loss of Pt active sites in acid media to obtain a better synergy between Pt and $CoWO_4$ (Co^{2+}). The carbon layer (NCL) covered on the WO_3-mr surface can improve the stability of WO_3, and provide the binding sites for $CoWO_4$ NPs (Co^{2+}). The interface between the mixed $CoWO_4$/WO_3 crystals can greatly promote the charge transfer during ORR.[44,59]

n CONCLUSION

In summary, we propose a simple route for the synthesis of $CoWO_4/WO_3$@NCL-mr as MOR/ORR co-catalyst/support. Oxygen vacancies on the $CoWO_4/WO_3$ can effectively adjust the surface electrons to thereby provide a stable anchoring location and surface for Pt attachment. The mass activity of Pt-$CoWO_4/WO_3$@ NCL-mr-850 (2208 mA mg$^{-1}_{Pt}$) is much higher than that of Pt/C (659.4 mA mg$^{-1}_{Pt}$). Meanwhile, the electrochemical stability of Pt-$CoWO_4/WO_3$@NCL-mr-850 is better than that of Pt/C in acidic media. The micro-rod structure of $CoWO_4/WO_3$@ NCL-mr exposes more Pt active sites to enhance the MOR activity/stability. In addition, H_xWO_3 generated on WO_3 is beneficial to improve the CO poisoning tolerance and MOR catalytic activity of Pt-$CoWO_4/WO_3$@NCL-mr-850 catalyst. Due to the strong interaction between Pt and carrier, Pt-$CoWO_4/WO_3$@NCL-mr-850 exhibits comparable ORR activity and stability to those of Pt/C. These findings provide a new strategy to prepare the microrod-structured catalysts with high electrocatalytic-activity by increasing the surface area and oxygen vacancies simultaneously.

n EXPERIMENTAL

Synthesis of ZIF-8 and ZIF-8@ZIF-67 Materials. For the synthesis of ZIF-8, 6.16 g (75 mmol) of 2-methylimidazole was dissolved in 150 mL of methanol, which was then added to a solution with 5.95 g (20 mmol) of $Zn(NO_3)_2{\cdot}6H_2O$ and 150 mL of methanol. The obtained white suspension was stood for 24 h at room temperature (25 ℃), and then was centrifugally washed with methanol for several times. The resulting white sample was dried overnight at 60 ℃ to obtain the product ZIF-8.[40,64]

For the synthesis of ZIF-8@ZIF-67, 0.5 g of the synthesized ZIF-8 was dispersed in 100 mL of methanol, and 5.82 g (20 mmol) of $Co(NO_3)_2{\cdot}6H_2O$ was dissolved in 100 mL of methanol. The above two solutions were thoroughly mixed together. Then, 6.16 g (75 mmol) of 2-methyl imidazole dissolved in 100 mL of methanol was poured into the above mixture to obtain the purple suspension with intense stirring at room temperature (25 ℃) for 24 h. After stirring, the suspension was stood for 24 h at 25 and the resulting precipitate was centrifuged and washed with methanol for at least three times. The purple sample was dried overnight at 60 ℃ to obtain the final product ZIF-8@ZIF-67.[40,64]

© 2022 fjirsm, CAS, Fuzhou

DOI: 10.14102/j.cnki.0254-5861.2022-0104

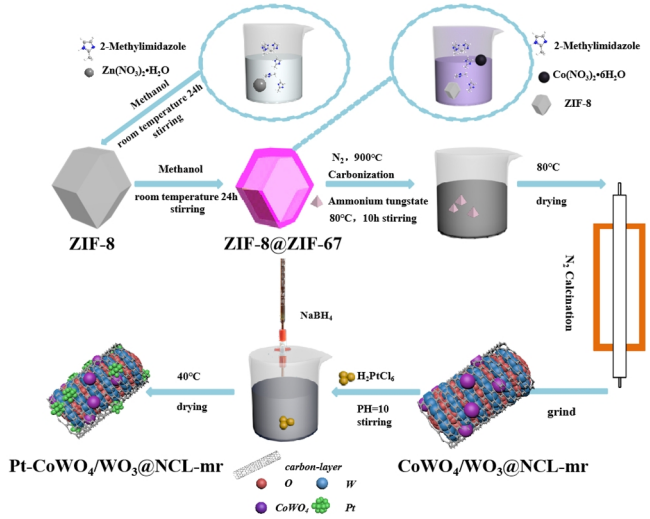

Scheme 2. Synthesis route for $CoWO_4/WO_3$@NCL-mr and Pt-$CoWO_4/WO_3$@NCL-mr composites.

Synthesis of $CoWO_4/WO_3$@NCL-mr. ZIF-8@ZIF-67 was carbonized at 900 °C to prepare the Co-NC composite. The obtained Co-NC was placed in a 5.0 M sulfuric acid (H_2SO_4) solution and stirred overnight, and then washed with deionized water until pH of the cleaning solution reached neutral. Co-NC was then mixed with 0.80 g of ammonium tungstate and 50 mL of deionized water, and the mixture was continuously stirred at 80 °C for 10 h under a water bath condition, and then dried at 80 °C. The dried mixture was separately heated from room temperature to 750, 800, 850, or 900 °C (5 °C min^{-1}) under N_2 atmosphere. The precursor was kept at the final temperature for 4 h, and then naturally cooled to room temperature (25 °C) in a N_2 atmosphere. The detailed preparation steps are shown in Scheme 2. The final samples were labeled as $CoWO_4/WO_3$@NCL-mr-X (X = 750, 800, 850, and 900). Material characterizations including XRD, XPS, N_2 adsorption/desorption isotherms, SEM, and TEM were introduced in the 'Supporting Information'. Methods for CV, LSV, electrochemical impedance spectroscopy, RRDE and CA tests were also introduced in the 'Supporting Information'.

n ACKNOWLEDGMENTS

We acknowledge the support by National Natural Science Foundation of China (52070074, 21806031 and 51578218) and LongJiang Scholars Program (Young Scholar, Q201912).

n AUTHOR INFORMATION

Corresponding authors. Emails: zjh_0308@126.com (Y. Dai), hlju_chem218c@163.com (Z. Cai) and zoujinlong@hlju.edu.cn (J. L. Zou).

n COMPETING INTERESTS

The authors declare no competing interests.

n ADDITIONAL INFORMATION

Supplementary information is available for this paper at http://manu30.magtech.com.cn/jghx/EN/10.14102/j.cnki.0254-5861.2022-0104

For submission: https://mc03.manuscriptcentral.com/cjsc

n REFERENCES

(1) Caglar, A.; Duzenli, D.; Onal, I.; Tersevin, I.; Sahin, O.; Kivrak, H. A comparative experimental and density functional study of glucose adsorption and electrooxidation on the Au-graphene and Pt-graphene electrodes. *Int. J. Hydrogen Energy* **2020**, 45, 490-500.

(2) Martinaiou, I.; Videla, A. H. A. M.; Weidler, N.; Kuebler, M.; Wallace, W. D. Z.; Paul, S.; Wagner, S.; Shahraei, A.; Stark, R. W.; Specchia, S.; Kramm, U. I. Activity and degradation study of an Fe-N-C catalyst for ORR in Direct Methanol Fuel Cell (DMFC). *Appl. Catal., B* **2020**, 262, 118217.

(3) Miao, B. Q.; Liu, Y. C.; Ding, Y.; Jin, P. J.; Chen, P.; Chen, Y. Rhodium nanodendrites catalyzed alkaline methanol oxidation reaction in direct methanol fuel cells. *Sustain. Mater. Technol.* **2022**, 31, e00379.

(4) Huang, W. J.; Wang, H. T.; Zhou, J. G.; Wang, J.; Duchesne, P. N.; Muir, D.; Zhang, P.; Han, N.; Zhao, F. P.; Zeng, M.; Zhong, J.; Jin, C. H.; Li, Y. G.; Lee, S. T.; Dai, H. J. Highly active and durable methanol oxidation electrocatalyst based on the synergy of platinum-nickel hydroxide-graphene. *Nat. Commun.* **2015**, 6, 10035.

(5) Zhao, Y.; Liu, Y.; Miao, B.; Ding, Y.; Jin, P.; Chen, Y. One-dimensional rhodium-nickel alloy assemblies with nano-dendrite subunits for alkaline methanol oxidation. *Chin. J. Struct. Chem.* **2022**, 41, 2204040-2204045.

(6) Brandon, N. P.; Skinner, S.; Steele, B. C. H. Recent advances in materials for fuel cells. *Annu. Rev. Mater. Res.* **2003**, 33, 183-213.

(7) Qin, C. L.; Fan, A. X.; Zhang, X.; Dai, X. P.; Sun, H.; Ren, D. H.; Dong, Z.; Wang, Y.; Luan, C. L.; Ye, J. Y.; Sun, S. G. The in situ etching assisted synthesis of Pt-Fe-Mn ternary alloys with high-index facets as efficient catalysts for electro-oxidation reactions. *Nanoscale* **2019**, 11, 9061-9075.

(8) Jin, Y. X.; Han, D. M.; Jia, W. P.; Li, F.; Chen, X. Y.; Huang, G. B.; Zhang, D. WO_3 modified graphene supported Pt electrocatalysts with enhanced performance for oxygen reduction reaction. *Int. J. Electrochem. Sci.* **2017**, 12, 6535-6544.

(9) Yu, Y.; You, S. J.; Du, J. N.; Xing, Z. P.; Dai, Y.; Chen, H.; Cai, Z.; Ren, N. Q.; Zou, J. L. ZIF-67-derived CoO (tetrahedral Co^{2+}) @nitrogen-doped porous carbon protected by oxygen vacancies-enriched SnO_2 as highly active catalyst for oxygen reduction and Pt co-catalyst for methanol oxidation. *Appl. Catal., B* **2019**, 259, 118043.

(10) Deng, K.; Xu, Y.; Yang, D. D.; Qian, X. Q.; Dai, Z. C.; Wang, Z. Q.; Li, X. N.; Wang, L.; Wang, H. J. Pt-Ni-P nanocages with surface porosity as efficient bifunctional electrocatalysts for oxygen reduction and methanol oxidation. *J. Mater. Chem. A* **2019**, 7, 9791-9797.

(11) Parthibavarman, M.; Karthik, M.; Prabhakaran, S. Facile and one step synthesis of WO_3 nanorods and nanosheets as an efficient photocatalyst and humidity sensing material. *Vacuum* **2018**, 155, 224-232.

(12) Wei, L. J.; Zhang, H. M.; Cao, J. Electrospinning of Ag/$ZnWO_4/WO_3$ composite nanofibers with high visible light photocatalytic activity. *Mater. Lett.* **2019**, 236, 171-174.

(13) Kuang, W. D.; Meng, X. J.; Wang, C. H.; Talluri, B.; Thomas, T.; Jiang, C. J.; Liu, S. Q.; Yang, M. H. Nitridation of $CoWO_4$/CdS nanocomposite formed metal nitrides assisting efficiently photocatalytic hydrogen evolution. *ACS Omega* **2020**, 5, 9969-9976.

(14) Jin, Z. L.; Yan, X.; Hao, X. Q. Rational design of a novel p-n heterojunction based on 3D layered nanoflower MoS_x supported $CoWO_4$

© 2022 fjirsm, CAS, Fuzhou

DOI: 10.14102/j.cnki.0254-5861.2022-0104

nanoparticles for superior photocatalytic hydrogen generation. *J. Colloid Interface Sci.* **2020**, 569, 34-49.

(15) Huang, B. R.; Hung, S. C.; Lin, C. Y.; Chen, Y. J. Effect of gas enhanced metal-semiconductor-metal UV photodetectors based on thermal annealing tungsten oxide thin film prepared by sol-gel method. *J. Mater. Sci.: Mater. Electron.* **2014**, 25, 408-413.

(16) Zhang, C. Y.; Dai, Y.; Chen, H.; Ma, Y. Y.; Jing, B. J.; Cai, Z.; Duan, Y. Q.; Tang, B.; Zou, J. L. Carbon-thin-layer protected WP with no passivation supported on acid-treated expanded graphite as efficient Pt Co-catalysts for methanol oxidation and oxygen reduction reactions. *J. Mater. Chem. A* **2018**, 6, 22636-22644.

(17) Guan, X. H.; Zhang, Z. W.; Yang, L.; Wang, G. S. One-pot hydrothermal synthesis of hexagonal WO_3 nanorods/graphene composites as high-performance electrodes for supercapacitors. *Chempluschem* **2017**, 82, 1174-1181.

(18) Xu, X. W.; Shen, J. F.; Li, N.; Ye, M. X. Facile synthesis of reduced graphene oxide/$CoWO_4$ nanocomposites with enhanced electrochemical performances for supercapacitors. *Electrochim. Acta* **2014**, 150, 23-34.

(19) Qu, F. D.; Zhang, N.; Zhang, S. D.; Zhao, R. Y.; Yao, D.; Ruan, S. P.; Yang, M. H. Construction of Co_3O_4/$CoWO_4$ core-shell urchin-like microspheres through ion-exchange method for high-performance acetone gas sensing performance. *Sens. Actuat., B* **2020**, 309, 127711.

(20) Zhao, Y. M.; Ikram, M.; Wang, J. Z.; Liu, Z.; Du, L. J.; Zhou, J.; Kan, K.; Zhang, W. J.; Li, L.; Shi, K. Y. Ultrafast NH_3 sensing properties of WO_3@$CoWO_4$ heterojunction nanofibres at room temperature. *Aust. J. Chem.* **2018**, 71, 87-94.

(21) Ferrari, P.; Molina, L. M.; Kaydashev, V. E.; Alonso, J. A.; Lievens, P.; Janssens, E. Controlling the adsorption of carbon monoxide on platinum clusters by dopant-induced electronic structure modification. *Angew. Chem. Int. Ed.* **2016**, 55, 11059-11063.

(22) Wang, A. L.; Liang, C. L.; Lu, X. F.; Tong, Y. X.; Li, G. R. Pt-MoO_3-RGO ternary hybrid hollow nanorod arrays as high-performance catalysts for methanol electrooxidation. *J. Mater. Chem. A* **2016**, 4, 1923-1930.

(23) Xia, B. Y.; Wu, H. B.; Chen, J. S.; Wang, Z.; Wang, X.; Lou, X. W. Formation of Pt-TiO_2-rGO 3-phase junctions with significantly enhanced electro-activity for methanol oxidation. *Phys. Chem. Chem. Phys.* **2012**, 14, 473-476.

(24) Georgieva, J.; Sotiropoulos, S.; Valova, E.; Armyanov, S.; Hubin, A.; Steenhaut, O.; Raes, M.; Papaderakis, A. Pt-doped TiO_2/WO_3 bi-layer catalysts on graphite substrates with enhanced photoelectrocatalytic activity for methanol oxidation under visible light, *J. Photochem. Photobiol., A* **2017**, 346, 70-76.

(25) Saha, M. S.; Banis, M. N.; Zhang, Y.; Li, R.; Sun, X.; Cai, M.; Wagner, F. T. Tungsten oxide nanowires grown on carbon paper as Pt electrocatalyst support for high performance proton exchange membrane fuel cells. *J. Power Sources* **2009**, 192, 330-335.

(26) Ye, J. L.; Liu, J. G.; Zou, Z. G.; Gu, J.; Yu, T. Preparation of Pt supported on WO_3-C with enhanced catalytic activity by microwave-pyrolysis method. *J. Power Sources* **2010**, 195, 2633-2637.

(27) Wu, Q.; Sheng, M.; Shi, J.; Zhou, Q.; Liao, F.; Lv, F. $CoWO_4$/CoP_2 nanoflakes grown on carbon nanotube film as an efficient electrocatalyst for water splitting in alkaline media. *Appl. Surf. Sci.* **2020**, 514, 145919.

(28) Duan, Y. Q.; Sun, Y.; Wang, L.; Dai, Y.; Chen, B.; Pan, S. Y.; Zou, J. L. Enhanced methanol oxidation and CO tolerance using oxygen-passivated molybdenum phosphide/carbon supported Pt catalysts. *J. Mater. Chem. A* **2016**, 4, 7674-7682.

(29) Saha, M.; Ghosh, S.; De, S. K. Nanoscale Kirkendall effect driven Au decorated CdS/CdO colloidal nanocomposites for efficient hydrogen evolution, photocatalytic dye degradation and Cr (VI) reduction. *Catal. Today* **2020**, 340, 253-267.

(30) Yi, Q. N.; Hu, C. G.; Yang, R. S.; Liu, H.; Wan, B. Y.; Zhang, Y. Preparation of WO_3 network squares for ultrasensitive photodetectors. *J. Alloys Compd*. **2011**, 509, L255-L261.

(31) Lei, Y.; Yang, F. W.; Si, Y. J.; Guo, C. Z.; Liu, J.; Li, M. J.; Xiong, Z. P. Boosting oxygen reduction catalysis with tailorable active-N-dominated doped defective CNTs. *Appl. Surf. Sci.* **2020**, 499, 143844.

(32) Han, Y. J.; Choi, K.; Oh, H.; Kim, C.; Jeon, D.; Lee, C.; Lee, J. H.; Ryu, J. Cobalt polyoxometalate-derived $CoWO_4$ oxygen-evolving catalysts for efficient electrochemical and photoelectrochemical water oxidation. *J. Catal.* **2018**, 367, 212-220.

(33) Xiao, E. C.; Liu, M.; Ren, Q.; Cao, Z.; Guo, M.; Dou, G.; Qi, Z. M.; Shi, F. Phonon characteristics and dielectric properties of a phase pure $CoWO_4$ ceramic. *Ceram. Int.* **2020**, 46, 15705-15708.

(34) Zhang, M. C.; Fan, H. Q.; Zhao, N.; Peng, H. J.; Ren, X. H.; Wang, W. J.; Li, H.; Chen, G. Y.; Zhu, Y. N.; Jiang, X. B.; Wu, P. 3D hierarchical $CoWO_4$/Co_3O_4 nanowire arrays for asymmetric supercapacitors with high energy density. *Chem. Eng. J.* **2018**, 347, 291-300.

(35) Xue, M. R.; Bao, X. L.; Li, X. Q.; Qin, L. X.; Han, S.; Kang, S. Z. A novel pathway toward efficient and stable C_3N_4-based photocatalyst for light driven H-2 evolution: the synergistic effect between Pt and $CoWO_4$. *Int. J. Hydrogen Energy* **2019**, 44, 28113-28122.

(36) Siller-Ceniceros, A. A.; Sanchez-Castro, M. E.; Morales-Acosta, D.; Torres-Lubian, J. R.; Martinez G, E.; Rodriguez-Varela, F. J. Innovative functionalization of Vulcan XC-72 with Ru organometallic complex: significant enhancement in catalytic activity of Pt/C electrocatalyst for the methanol oxidation reaction (MOR). *Appl. Catal., B* **2017**, 209, 455-467.

(37) Prabavathi, S. L.; Govindan, K.; Saravanakumar, K.; Jang, A.; Muthuraj, V. Construction of heterostructure $CoWO_4$/g-C_3N_4 nanocomposite as an efficient visible-light photocatalyst for norfloxacin degradation. *J. Ind. Eng. Chem.* **2019**, 80, 558-567.

(38) Bock, D. C.; Ou, N. C.; Bonsu, R. O.; Anghel, C. T.; Su, X.; McElwee-White, L. Synthesis of tungsten oxo fluoroalkoxide complexes $WO(OR)_3L$ as precursors for growth of WO_x nanomaterials by aerosol-assisted chemical vapor deposition. *Solid State Ionics* **2018**, 315, 77-84.

(39) Zhang, W. M.; Yue, Z. W.; Wang, Q. M.; Zeng, X. X.; Fu, C. C.; Li, Q.; Li, X. T.; Fang, L. D.; Li, L. Carbon-encapsulated CoS_2 nanoparticles anchored on N-doped carbon nanofibers derived from ZIF-8/ZIF-67 as anode for sodium-ion batteries. *Chem. Eng. J.* **2020**, 380, 122548.

(40) Chen, H.; You, S. J.; Ma, Y. Y.; Zhang, C. Y.; Jing, B. J.; Cai, Z.; Tang, B.; Ren, N. Q.; Zou, J. L. Carbon thin-layer-protected active sites for ZIF-8-derived nitrogen-enriched carbon frameworks/expanded graphite as metal-free catalysts for oxygen reduction in acidic media. *Chem. Mater.* **2018**, 30, 6014-6025.

(41) Dong, H. F.; Zhao, Y.; Tang, Y. F.; Burkert, S. C.; Star, A. Oxidative unzipping of stacked nitrogen-doped carbon nanotube cups. *ACS Appl. Mater. Interfaces* **2015**, 7, 10734-10741.

(42) Shi, P. C.; Yi, J. D.; Liu, T. T.; Li, L.; Zhang, L. J.; Sun, C. F.; Wang, Y. B.; Huang, Y. B.; Cao, R. Hierarchically porous nitrogen-doped carbon nanotubes derived from core-shell ZnO@zeolitic imidazolate framework nanorods for highly efficient oxygen reduction reactions. *J. Mater. Chem. A* **2017**, 5, 12322-12329.

(43) Zhong, H. X.; Wang, J.; Zhang, Q.; Meng, F.; Bao, D.; Liu, T.; Yang, X.

© 2022 fjirsm, CAS, Fuzhou

DOI: 10.14102/j.cnki.0254-5861.2022-0104

Y.; Chang, Z. W.; Yan, J. M.; Zhang, X. B. In situ coupling FeM (M = Ni, Co) with nitrogen-doped porous carbon toward highly efficient trifunctional electrocatalyst for overall water splitting and rechargeable Zn-air battery. *Adv. Sustain. Syst.* **2017**, 1, 2366-7486.

(44) Jeyakanthan, M.; Subramanian, U.; Tangsali, R. B.; Ramesh, A. AC conductivity, electrochemical and magnetic studies of $CoWO_4$/$PbWO_4$ nanocomposites. *Phys. B* **2020**, 586, 412151.

(45) Jayaraman, S.; Jaramillo, T. F.; Baeck, S. H.; McFarland, E. W. Synthesis and characterization of Pt-WO_3 as methanol oxidation catalysts for fuel cells. *J. Phys. Chem. B* **2005**, 109, 22958-66.

(46) Mohamed, M. M.; Khairy, M.; Eid, S. Polyethylene glycol assisted one-pot hydrothermal synthesis of $NiWO_4$/WO_3 heterojunction for direct methanol fuel cells. *Electrochim. Acta* **2018**, 263, 286-298.

(47) Li, J. H.; You, S. J.; Liu, M. Y.; Zhang, P.; Dai, Y.; Yu, Y.; Ren, N. Q.; Zou, J. L. ZIF-8-derived carbon-thin-layer protected WC/$W_{24}O_{68}$ micro-sized rods with enriched oxygen vacancies as efficient Pt co-catalysts for methanol oxidation and oxygen reduction. *Appl. Catal., B* **2020**, 265, 0926-3373.

(48) Yoon, D.; Manthiram, A. Hydrogen tungsten bronze as a decoking agent for long-life, natural gas-fueled solid oxide fuel cells. *Energy Environ. Sci*. **2014**, 7, 3069-3076.

(49) Du, X. W.; Luo, S. P.; Du, H. Y.; Tang, M.; Huang, X. D.; Shen, P. K. Monodisperse and self-assembled Pt-Cu nanoparticles as an efficient electrocatalyst for the methanol oxidation reaction. *J. Mater. Chem. A* **2016**, 4, 1579-1585.

(50) Li, F.; Gong, H. Y.; Wang, Y.; Zhang, H.; Wang, Y. Z.; Liu, S. N.; Wang, S.; Sun, C. W. Enhanced activity, durability and anti-poisoning property of Pt/$W_{18}O_{49}$ for methanol oxidation with a sub-stoichiometric tungsten oxide $W_{18}O_{49}$ support. *J. Mater. Chem. A* **2014**, 2, 20154-20163.

(51) Zhang, Z.; Liu, J.; Gu, J.; Su, L.; Cheng, L. An overview of metal oxide materials as electrocatalysts and supports for polymer electrolyte fuel cells. *Energy Environ. Sci*. **2014**, 7, 2535-2558.

(52) Jassal, A. K.; Mudsainiyan, R. K.; Shankar, R. A rational assembly of paradodecatungstate anions from clusters to morphology-controlled nanomaterials. *Mater. Chem. Front.* **2021**, 5, 1090-1125.

(53) Calderona, J. C.; Garcia, G.; Calvillo, L.; Rodriguez, J. L.; Lazaro, M. J.; Pastor, E. Electrochemical oxidation of CO and methanol on Pt-Ru catalysts supported on carbon nanofibers: the influence of synthesis method. *Appl. Catal., B* **2015**, 165, 676-686.

(54) Kim, I. T.; Choi, M.; Lee, H. K.; Shim, J. Characterization of methanol-tolerant Pd-WO_3 and Pd-SnO_2 electrocatalysts for the oxygen reduction reaction in direct methanol fuel cells. *J. Ind. Eng. Chem.* **2013**, 19, 813-818.

(55) Zhao, Z. G.; Yao, Z. J.; Zhang, J.; Zhu, R.; Jin, Y.; Li, Q. W. Rational design of galvanically replaced Pt-anchored electrospun WO_3 nanofibers as efficient electrode materials for methanol oxidation. *J. Mater. Chem.* **2012**, 22, 16514-16519.

(56) Wang, W. C.; Li, X.; He, T. O.; Liu, Y. M.; Jin, M. S. Engineering surface structure of Pt nanoshells on Pd nanocubes to preferentially expose active surfaces for ORR by manipulating the growth kinetics. *Nano Lett.* **2019**, 19, 1743-1748.

(57) Yu, Y.; You, S. J.; Du, J.; Zhang, P.; Dai, Y.; Liu, M. Y.; Jiang, B. J.; Ren, N. Q.; Zou, J. L. Ti^{3+}-self-doped TiO_2 with multiple crystal-phases anchored on acid-pickled ZIF-67-derived Co_3O_4@N-doped graphitized-carbon as a durable catalyst for oxygen reduction in alkaline and acid media. *Chem. Eng. J.* **2021**, 403, 126441.

(58) Ganguly, A.; Anjaneyulu, O.; Ojha, K.; Ganguli, A. K. Oxide-based nanostructures for photocatalytic and electrocatalytic applications. *Crystengcomm* **2015**, 17, 8978-9001.

(59) Song, D. H.; Shin, J.; Lee, Y. J.; Kwon, Y.; Lim, J.; Kim, E. J.; Oh, S.; Kim, M.; Cho, E. Thin nickel layer with embedded WC nanoparticles for efficient oxygen evolution. *ACS Appl. Energy Mater.* **2019**, 2, 3452-3460.

(60) Rajpurohit, A. S.; Punde, N. S.; Rawool, C. R.; Srivastava, A. K. Fabrication of high energy density symmetric supercapacitor based on cobalt-nickel bimetallic tungstate nanoparticles decorated phosphorus-sulphur co-doped graphene nanosheets with extended voltage. *Chem. Eng. J.* **2019**, 371, 679-692.

(61) Liu, J. F.; Zhang, Z. F.; Wang, Z.; Tang, M. Y.; Li, J. Q.; Yi, J. H.; Zuo, T. Y.; Wu, Y. F.; Ma, Q. B. Flower-like WO_3/$CoWO_4$/Co nanostructures as high performance anode for lithium ion batteries. *J. Alloys Compd.* **2017**, 727, 107-113.

(62) Elrouby, M.; Abd El-Lateef, H. M.; Sadek, M. Electrodeposited Pt nanorods on a novel flowered-like nanostructured Ni-Co alloy as an electrocatalyst for methanol oxidation. *Int. J. Hydrogen Energy* **2019**, 44, 13820-13834.

(63) Yang, C.; van der Laak, N. K.; Chan, K. Y.; Zhang, X. Microwave-assisted microemulsion synthesis of carbon supported Pt-WO_3 nanoparticles as an electrocatalyst for methanol oxidation. *Electrochim. Acta* **2012**, 75, 262-272.

(64) Pan, Y.; Sun, K.; Liu, S.; Cao, X.; Wu, K.; Cheong, W. C.; Chen, Z.; Wang, Y.; Li, Y.; Liu, Y.; Wang, D.; Peng, Q.; Chen, C.; Li, Y. Core-shell ZIF-8@ZIF-67-derived CoP nanoparticle-embedded N-doped carbon nanotube hollow polyhedron for efficient overall water splitting. *J. Am. Chem. Soc.* **2018**, 140, 2610-2618.

Received: May 22, 2022
Accepted: June 12, 2022
Published online: June 20, 2022
Published: July 18, 2022

© 2022 fjirsm, CAS, Fuzhou

DOI: 10.14102/j.cnki.0254-5861.2022-0104